REPORT DOCUMENTATION PAGE

Form Approved
OMB No. 0704-0188

Public reporting burden for this collection of information is estimated to average 1 hour per response, including the time for reviewing instructions, searching existing data sources, gathering and maintaining the data needed, and completing and reviewing this collection of information. Send comments regarding this burden estimate or any other aspect of this collection of information, including suggestions for reducing this burden to Department of Defense, Washington Headquarters Services, Directorate for Information Operations and Reports (0704-0188), 1215 Jefferson Davis Highway, Suite 1204, Arlington, VA 22202-4302. Respondents should be aware that notwithstanding any other provision of law, no person shall be subject to any penalty for failing to comply with a collection of information if it does not display a currently valid OMB control number. **PLEASE DO NOT RETURN YOUR FORM TO THE ABOVE ADDRESS.**

1. REPORT DATE *(DD-MM-YYYY)*	**2. REPORT TYPE**	**3. DATES COVERED** *(From - To)*
June 2013	Technical Paper	June 2013-July 2013

4. TITLE AND SUBTITLE
Influence of Boundary Condition Treatment on Longitudinal Mode Combustion Instability Predictions

5a. CONTRACT NUMBER
In-House

5b. GRANT NUMBER

5c. PROGRAM ELEMENT NUMBER

6. AUTHOR(S)
Harvazinski, M. , Talley, D., and Sankaran, V.

5d. PROJECT NUMBER

5e. TASK NUMBER

5f. WORK UNIT NUMBER
Q0A1

7. PERFORMING ORGANIZATION NAME(S) AND ADDRESS(ES)

Air Force Research Laboratory (AFMC)
AFRL/RQRC
10 E. Saturn Blvd.
Edwards AFB CA 93524-7680

8. PERFORMING ORGANIZATION REPORT NO.

9. SPONSORING / MONITORING AGENCY NAME(S) AND ADDRESS(ES)
Air Force Research Laboratory (AFMC)
AFRL/RQR
5 Pollux Drive
Edwards AFB CA 93524-7048

10. SPONSOR/MONITOR'S ACRONYM(S)

11. SPONSOR/MONITOR'S REPORT NUMBER(S)
AFRL-RQ-ED-TP-2013-156

12. DISTRIBUTION / AVAILABILITY STATEMENT
Distribution A: Approved for Public Release; Distribution Unlimited. PA#13361

13. SUPPLEMENTARY NOTES
Conference paper for the 49th AIAA/ASME/SAE/ASEE Joint Propulsion Conference, San Jose, CA, 15-17 July 2013.

14. ABSTRACT
Combustion instability in rocket chambers is strongly influenced by acoustic interactions at the boundaries of the configuration. Many CFD simulations employ approximate boundary conditions in order to simplify the geometry but the impact that they have on the solution is not well understood. The present study focuses on the use of detailed (exact) boundary representations and an approximate boundary condition in a given longitudinal mode test chamber. The actual inlet boundary of the injector is comprised of a series of choked slots while the approximate boundary condition is a uniform constant mass flow. Both two and three-dimensional simulations are carried out. Differences in the flowfield are evident in the combustion region away from the inlet, including the size of the recirculation region and location of the peak heat release. The amplitudes of the acoustic modes are well predicted for the first two modes especially in three-dimensional simulation, while higher modes are poorly predicted. These results suggest that such boundary condition approximations must be judiciously used and having access to more detailed treatments is important to verify accuracy.

15. SUBJECT TERMS

16. SECURITY CLASSIFICATION OF:			**17. LIMITATION OF ABSTRACT**	**18. NUMBER OF PAGES**	**19a. NAME OF RESPONSIBLE PERSON**
					Doug Talley
a. REPORT	**b. ABSTRACT**	**c. THIS PAGE**	SAR	15	**19b. TELEPHONE NO** *(include area code)*
Unclassified	**Unclassified**	**Unclassified**			661-525-6174

Standard Form 298 (Rev. 8-98)
Prescribed by ANSI Std. 239.18

Influence of Boundary Condition Treatment on Longitudinal Mode Combustion Instability Predictions

Matthew E. Harvazinski*, Douglas G. Talley†, Venkateswaran Sankaran‡
Air Force Research Laboratory, Edwards AFB, CA, 93524

Combustion instability in rocket chambers is strongly influenced by acoustic interactions at the boundaries of the configuration. Many CFD simulations employ approximate boundary conditions in order to simplify the geometry but the impact that they have on the solution is not well understood. The present study focuses on the use of detailed (exact) boundary representations and an approximate boundary condition in a given longitudinal mode test chamber. The actual inlet boundary of the injector is comprised of a series of choked slots while the approximate boundary condition is a uniform constant mass flow. Both two and three-dimensional simulations are carried out. Differences in the flowfield are evident in the combustion region away from the inlet, including the size of the recirculation region and location of the peak heat release. The amplitudes of the acoustic modes are well predicted for the first two modes especially in three-dimensional simulation, while higher modes are poorly predicted. These results suggest that such boundary condition approximations must be judiciously used and having access to more detailed treatments is important to verify accuracy.

Nomenclature

f	Frequency
p'	Pressure fluctuation
p'_{ptp}	Peak-to-peak pressure fluctuation
p_{rms}	RMS pressure fluctuation
$\dot{q}'$	Heat release fluctuations
$\mathscr{R}$	Rayleigh index

I. Introduction

Rocket engines contain a wide range of length scales. Injector passages can be micrometers in size while combustor diameters and lengths may be on the order of a meter (or less). The ability to resolve these length scales while producing a high quality mesh with a reasonable number of grid points is a challenge. The approximation of the small injector features has the potential to greatly reduce the time required to produce the mesh as well as save substantially on the computational time. However, the effects of such geometric approximations are not always well understood and their impact on phenomena of importance in rocket engines such as combustion-acoustic coupling can be significant. The present study looks at the effect of the inlet boundary condition of a single-element injector on the stability characteristics of an unstable laboratory rocket engine.

For a single-element injector, modeling the entire geometry including the injector details is possible. However, geometric approximations are necessary for the simulation of a full-scale rocket engine. Where there can be 100's or 1000's of geometrically complex injector elements. A simulation of such a configuration is almost impossible when the full geometry of each injector is required. The use of approximate boundary

*Scientist, AIAA Member.
†Research Physical Scientist, AIAA Associate Fellow.
‡Senior Scientist, AIAA Member.

Distribution Statement A: Approved for public release; distribution is unlimited.

conditions has the potential to reduce the number of grid points by as much as an order of magnitude. Such a reduction in problem size can therefore make the simulation of a full-scale rocket engine more tractable. It is however critical that any approximation of the boundary condition does not impact the accuracy of the acoustic modes in the chamber or the stability characteristics of the engine.

The test configuration considered here is the longitudinal-mode continuously variable resonance chamber (CVRC) experiment conducted at Purdue University. The CVRC experiment originally developed by Yu et al. exhibits both stable and unstable combustion regimes. The variable levels of instability are achieved by varying the oxidizer post length.[1] The length of the oxidizer post is varied from 3.5 in to 7.5 in (8.89 cm to 19.05 cm). The combustion is stable at the short and long lengths and unstable between them. The length of the combustor remains fixed at 15 in (38.1 cm). For the purpose of this study three fixed oxidizer post lengths are considered, 3.5 in (8.89 cm), 5.5 in (13.97 cm), and 7.5 in (19.05 cm), the short and long lengths correspond to stable operating points and the middle length corresponds to an unstable configuration.

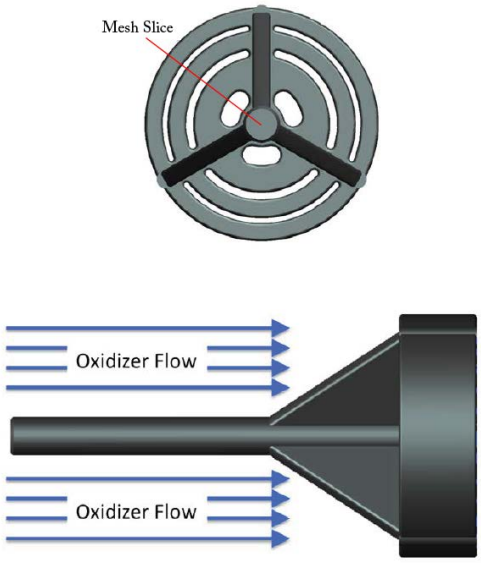

(a) Experimental oxidizer injector.[2]

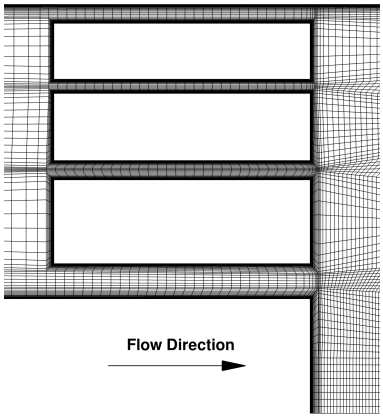

(b) Slice of the mesh required for the slots taken along the line in (a).

Figure 1: Geometrically complex oxidizer injector.

The oxidizer inlet boundary condition is problematic because of its geometric complexity. The oxidizer, 90% decomposed hydrogen peroxide, flows through an injector which is made up of three concentric slots. A fourth gap arises from the spacing between the injector and the outer wall of the oxidizer post, the injector is shown in Figure 1. The oxidizer flow through these slots is choked in order to isolate the combustor acoustics from the oxidizer manifold, which enables the experimental system to be more easily characterized and allows the computational simulations to exclude the fluid dynamics and acoustics in the manifold. The slotted geometry however presents a challenge for the construction of the mesh and increases the total grid point count. The smallest slot has a width of just 0.016 in which is small compared with the diameter of the oxidizer post, 0.769 in. The need to resolve the boundary layer around each of these slots adds significant complexity to the grid generation and increases the number of mesh points required. A two-dimensional slice showing the grid required for the slots is shown in Figure 1.

A commonly used alternative to the choked slots inlet is a uniform mass flow boundary condition. This greatly reduces the complexity of the grid and reduces the mesh size by about 20%. This reduction in the problem size is significant for combustion instability simulations which are unsteady and have long simulation times. While it is convenient to replace the choked slots with a uniform inlet, the impact of this change on the chamber acoustics and the stability characteristics of the longitudinal chamber is not well understood. Figure 2 shows the static pressure and vorticity near the slots from a previous three-dimensional simulation.[3] At the instant in time shown a high-pressure pulse has just reflected off the inlet and is now moving downstream away from the slots. Adjacent to the slots is a region of lower pressure resulting from the shed vortices. Both quantities show the unsteady nature of the flow in this region.

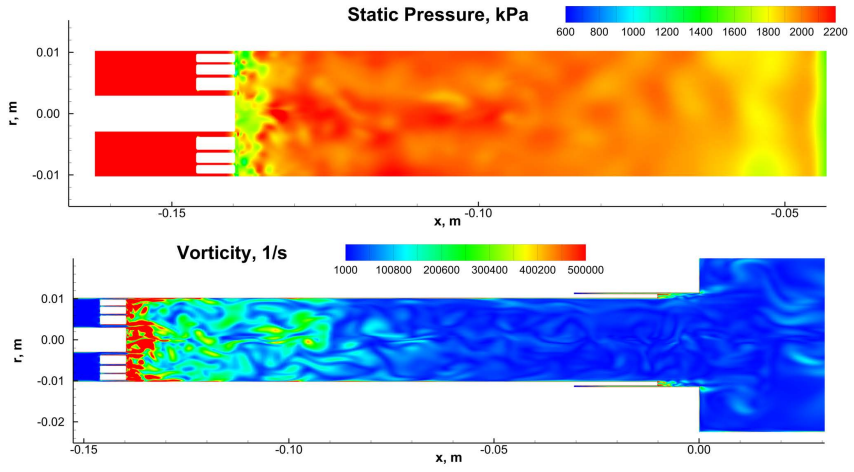

Figure 2: Instantaneous flowfield near the slots showing the static pressure (top) and vorticity (bottom).

The purpose of this work is to evaluate the impact of the inlet boundary condition on the stability characteristics of the longitudinal chamber. To gain the best understanding, both boundary conditions are simulated for a single operating condition using the same code. This provides the best opportunity to make side-by-side comparisons. It is already known that the flowfield near the slots is different, so the main focus is on the differences in the predicted amplitude and frequency of the unstable acoustic modes.

II. Previous Work

Two operating conditions were simulated in three-dimensions by Harvazinski et al. and Feldman et al. using a geometry that included the choked inlet slots. These results showed that the flowfield around the slots was highly unsteady and featured a large amount of vorticity generated from vortices shed from the slot walls. The simulations also compared well with experimental results of the acoustic modes.[3–5] A number of two-dimensional simulations were done by Smith et al. which also showed a large amount of unsteadiness near the slots.[6,7] Work by Garby et al. ignored the slots and replaced the boundary with a constant mass flow inlet. Unstable behavior was exhibited for the single operating point simulated.[8] Work by Guézennec et al. simulated the same condition as Garby also ignoring the slots and also predicted unstable combustion.[9] The effect of the boundary condition change is difficult to assess given the different codes and different physical models used in these studies.

III. Computational Model

The GEMS CFD code developed at Purdue University is used for the present simulations.[10–13] GEMS is a finite-volume based code that is second order accurate in both time and space. An implicit formulation is used which allows for the use of high-aspect ratio grids near the wall to resolve the boundary layer. A dual-time scheme is used to reduce approximate factorization errors in the implicit formulation. Turbulence is accounted for using a hybrid RANS/LES formulation that allows the code to operate in LES mode where the grid resolution supports it and in RANS mode where it does not, in particular the near wall region.[14,15] The two-equation k-ω turbulence model is used for the under resolved regions.[16,17]

The complete computational domain including the slots is shown in Figure 3. Decomposed hydrogen peroxide is used as the oxidizer and gaseous methane is used as the fuel. Combustion is modeled using a single step global reaction for the three-dimensional simulations[18] and a four-step reduced mechanism for the axisymmetric simulations.[19] The single step global reaction is,

$$CH_4 + 2\,O_2 \longrightarrow 2\,H_2O + CO_2 \tag{1}$$

The use of a global reaction minimizes the number of species that must be determined in the coupled system while retaining the pressure dependence of the reaction rate, which is critical for capturing the combustion-

acoustic coupling. The four-step mechanism is,

$$2\,CH_4 + O_2 \longrightarrow 2\,CO + 4\,H_2 \tag{2}$$
$$CH_4 + H_2O \longrightarrow CO + 3\,H_2 \tag{3}$$
$$2\,H_2 + O_2 \longrightarrow H_2O \tag{4}$$
$$CO + H_2O \longrightarrow CO_2 + H_2. \tag{5}$$

By supplementing the global reactions (eq. 2, 3) with equilibrium reactions (eq. 4, 5), more realistic physics are added to the global reaction "black box" combustion model.

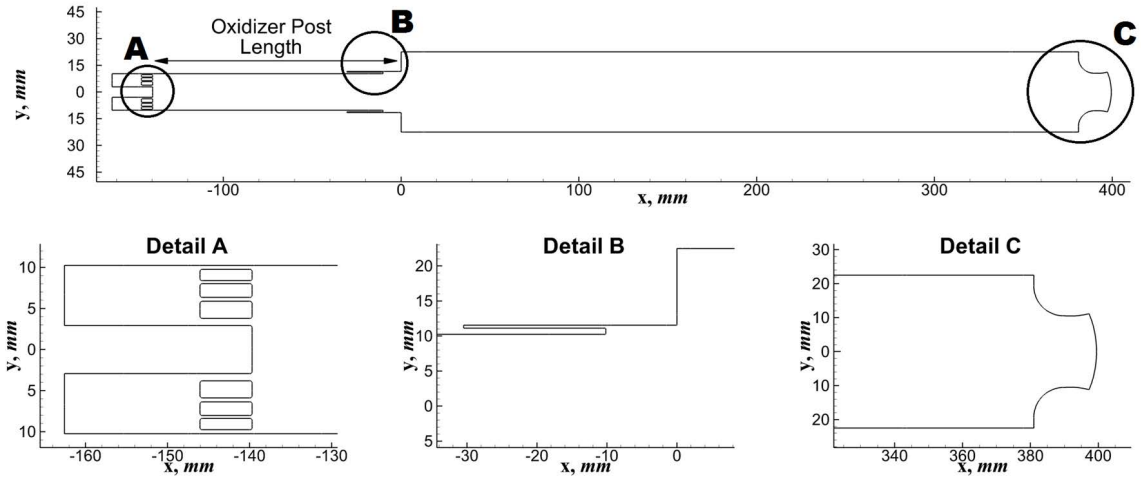

Figure 3: Combustor geometry showing the oxidizer inlet (detail A), fuel inlet (detail B), and the converging diverging nozzle (detail C).

Due to the large number of cases required to capture the effect of oxidizer post length for the choked slots and uniform mass flow inlet configurations two-dimensional simulations are used in combination with a limited number of three-dimensional simulations. A previous study by Harvazinski et al. showed that two-dimensional axisymmetric simulations using the choked slots were able to capture at least the first mode of instability but predicted a lower overall level of instability than was experimentally observed (and predicted by the three-dimensional simulations).[4] A similar difference in the predicted instability magnitude between two and three-dimensional simulations was also reported by Garby et al.[8]

Eight simulations have been completed to study the influence of the inlet boundary condition. Six simulations, cases 1-6, are two-dimensional axisymmetric calculations and form a parametric study of the oxidizer post length and the inlet boundary condition. The remaining two simulations are three-dimensional, cases 7 and 8, and simulate the 5.5 in oxidizer post length. The configuration of each simulation is summarized in Table 1.

The flowfield is initialized with hot (1500 K) combustion products in the combustor and oxidizer at the inlet temperature (1030 K) in the oxidizer tube. The simulations are started at quiescent conditions, and at the start of the simulation, diaphragms at the inlets and nozzle exit are broken allowing the flowfield to establish. Ignition takes place nominally two milliseconds after the start. The two-dimensional simulations are run for 100 ms and three-dimensional simulations are run for 40 ms. Two-dimensional simulations are observed to have a longer initial transient whereas three-dimensional simulations quickly lock onto the unstable mode after ignition. Two-dimensional simulations used 64 CPU cores while three-dimensional simulations were run with 960 CPU cores.

IV. Experimental Results

Different levels of instability are observed experimentally when the oxidizer post length is changed. At the start of the experiment, the oxidizer post length is 7.5 in, and during the test the oxidizer post length is gradually reduced to 3.5 in. Fixed length, forward translating, and backward translating tests all exhibit similar amplitudes for the three discrete lengths chosen for this investigation. A power spectral density

Table 1: Summary of simulation conditions.

Case	Oxidizer Post Length, in	Dimension	Chemical Kinetic Model	Inlet Boundary Condition
1	3.5	2D	Four Step	Choked Slots
2	5.5	2D	Four Step	Choked Slots
3	7.5	2D	Four Step	Choked Slots
4	3.5	2D	Four Step	Uniform Mass Flow
5	5.5	2D	Four Step	Uniform Mass Flow
6	7.5	2D	Four Step	Uniform Mass Flow
7	5.5	3D	Single Step	Choked Slots
8	5.5	3D	Single Step	Uniform Mass Flow

(PSD) analysis of three operating points, 3.5 in, 5.5 in, and 7.5 in is shown in Figure 4. It is clear from the figure that the 5.5 in case is the most unstable and the 7.5 in case is stable. The amplitude of the 3.5 in length falls between the other two results, showing a lower level for the first mode and less overall excitation of the higher order modes.

A quantitative analysis of the PSD is summarized in Table 2. The table shows the frequency of the first three modes and the corresponding peak-to-peak pressure amplitudes. To find the peak-to-peak pressure amplitudes the region under the PSD peaks is integrated using the full-width half-max (FWHM) method, this determines the root mean square (rms) pressure. The peak-to-peak pressure is then related to the rms pressure by,

$$p'_{\text{ptp}} = 2\sqrt{2}p_{\text{rms}}. \tag{6}$$

It should be noted that experimentally the transition from unstable to stable is close to the 7.5 in length and occurs very suddenly. Moreover, when the first 5 in of the metal combustion chamber is replaced with a quartz/acrylic optical section (mimicking an adiabatic wall) the transition to stable combustion is observed to occur almost precisely at 7.5 in.

Table 2: Frequency and peak-to-peak pressure amplitudes for the experimental operating points.

Oxidizer Post Length, in	Mode	f, Hz	p'_{ptp}, kPa
3.5	1	1379	121.17
	2	2734	5.86
	3	3882	16.03
5.5	1	1324	387.15
	2	2655	89.29
	3	3979	46.37
7.5	1	1220	15.57
	2	3650	8.10
	3	–	–

V. Two-dimensional Parametric Study

A PSD analysis using a pressure time history from a point on the combustor wall located 14.5 in downstream from the backstep was performed on the data from the six two-dimensional cases. The location of the pressure measurement point corresponds to the experimental pressure transducer location that was used to generate the experimental PSDs shown in Figure 4. The analysis used the final 60 ms of data with a sample rate of 1×10^7 Hz. This provides a frequency resolution of 16.7 Hz and a maximum frequency of 5000 kHz, well above the frequencies of interest ($1 - 6$ kHz). The PSD plot for each case is shown in Figure 5 and a qualitative interrogation of the PSDs is summarized in Table 3. The peak-to-peak pressure amplitude is again determined using the FWHM method.

The spectral analysis shows substantial differences between the cases, both in amplitude and frequencies. For the 3.5 in oxidizer post length both simulations under-predict the amplitude of the first mode, which is typical of two-dimensional simulations. Both inlet conditions do an excellent job predicting the frequency of the first mode, with the slotted configuration performing slightly better. For the second mode the frequencies

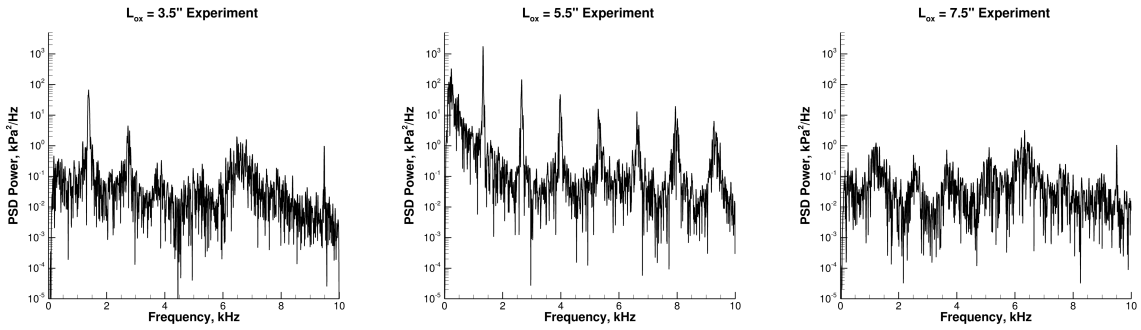

(a) 3.5 in (b) 5.5 in (c) 7.5 in

Figure 4: PSD analysis for the experimental operating conditions cases, point of analysis is on the wall 14.5 in downstream from the backstep.

are off for both inlets, and the amplitudes are over predicted. The slotted inlet actually identifies the second mode as the dominant mode. Frequency identification of the second and third mode is poor.

The unstable case, 5.5 in, is found to be unstable for both inlets but the constant mass flow case predicts a substantially higher level of amplitude, although still low compared to the experiment. Also, the frequencies are different for the two inlets, both being higher than the experimental value. The frequencies of the higher modes are similarly in poor agreement with the corresponding experimental values.

The simulations for the 7.5 in oxidizer post length are also not in good agreement with the experimental data. This should be a stable operating point but both inlet conditions predict an unstable mode. For the case without slots the amplitude is higher than the unstable 5.5 in length. As was mentioned in the experimental description the 7.5 in operating condition is close to the unstable operating point. The approximations made for these simulations: adiabatic walls, axisymmetric boundary conditions, and simplified kinetics (which give approximate molecular weights, sound speeds, and mean pressures) are likely the culprits for the poor prediction.

In summary, the two-dimensional simulations can at best reproduce some of the qualitative features of the stability characteristics. The lack of qualitative agreement with the experimental predictions makes it difficult to evaluate the efficacy of the approximate inlet boundary treatment. These results suggest that it may be necessary to employ full three-dimensional simulations to elucidate quantitative trends.

Table 3: Frequency and peak-to-peak pressure amplitudes.

(a) Slots.

Case	Mode	f, Hz	p'_{ptp}, kPa
1, 3.5 in	1	1383	16.103
	2	2917	23.400
	3	4200	15.447
2, 5.5 in	1	1550	49.304
	2	2583	15.123
	3	4000	4.979
3, 7.5 in	1	1383	34.416
	2	2800	10.343
	3	4333	9.696

(b) No Slots.

Case	Mode	f, Hz	p'_{ptp}, kPa
4, 3.5 in	1	1417	27.964
	2	2683	21.422
	3	3050	10.654
5, 5.5 in	1	1467	135.656
	2	2950	14.028
	3	4167	10.340
6, 7.5 in	1	1383	155.971
	2	2767	48.203
	3	3983	5.134

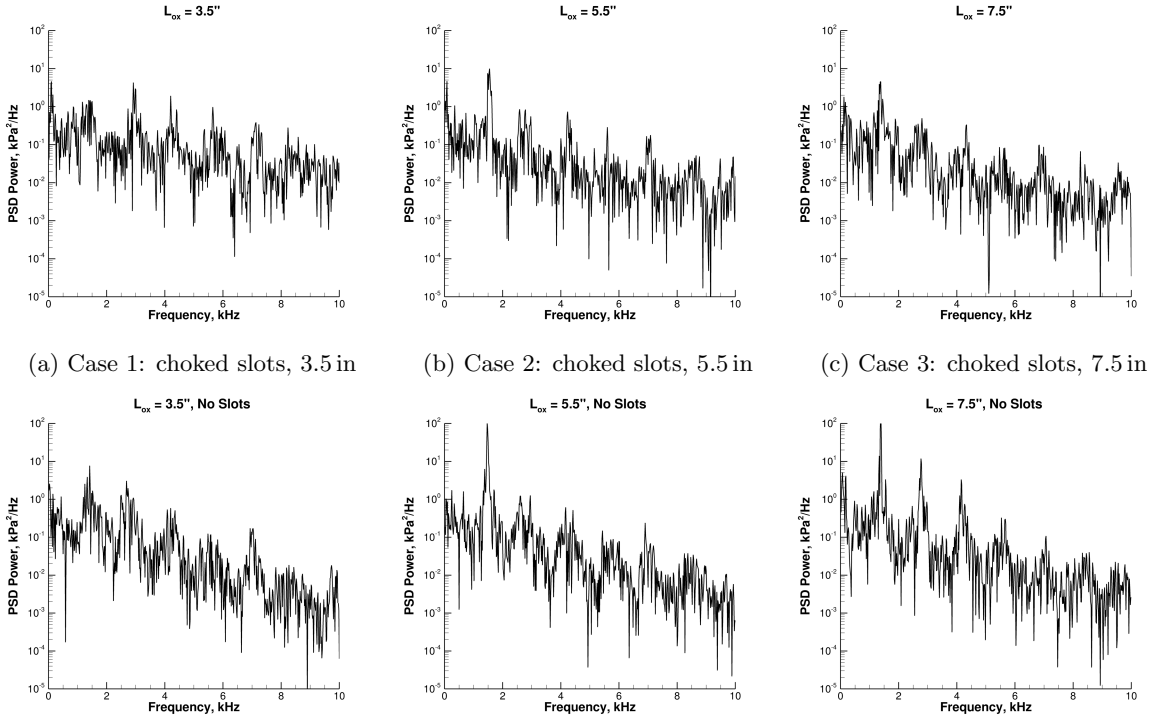

(a) Case 1: choked slots, 3.5 in (b) Case 2: choked slots, 5.5 in (c) Case 3: choked slots, 7.5 in

(d) Case 4: no slots, 3.5 in (e) Case 5: no slots, 5.5 in (f) Case 6: no slots, 7.5 in

Figure 5: PSD analysis for the six two-dimensional cases, point of analysis is 14.5 in downstream from the backstep.

VI. Three-dimensional Results

A. Instability Amplitude and Frequency Content

A PSD analysis has been performed using the data from the three-dimensional simulations. The analysis uses the final 35 ms of data which has a sample rate of 1×10^7 Hz. This provides a frequency resolution of 28.5 Hz and a maximum frequency of 5000 kHz. The PSDs are shown in Figure 6 and a qualitative interrogation of the PSDs is summarized in Table 4. Unlike the two-dimensional simulations, the three-dimensional simulations predict peak-to-peak pressures that are far closer to the experimental values.

For the first two modes the simulations with and without the slots produce identical frequencies, (at least within ± 28 Hz resolution available in the PSD analysis). For the third mode, the case without slots produces a lower frequency which is not a higher harmonic of the fundamental mode. For both the experiment and choked slots simulation, the third mode frequency is nearly three times the first mode, i.e. 3.01 and 2.98 respectively. On the other hand the frequency predicted by the constant mass flow case is 2.75 times the first mode frequency. Thus, the more approximate constant mass flow boundary condition is unable to correctly replicate the higher order harmonic behavior that is observed experimentally.

The choked slots case under-predicts the primary mode amplitude but is able to closely predict the next two modes. The constant mass flow case predicts higher amplitudes for the first two modes, but under-predicts the third mode. Overall, the predicted instability levels are higher for this approximate boundary condition.

B. Waveform

Snapshots of the unsteady pressure are shown in Figure 7. Again, it appears that the overall amplitude of the constant mass flow simulation is higher which is consistent with the PSD analysis. The phase difference in the plots is insignificant and is simply the result of slight differences in the ignition time and initial transient. Both simulations show the characteristic steep fronted waves observed in combustion instability.

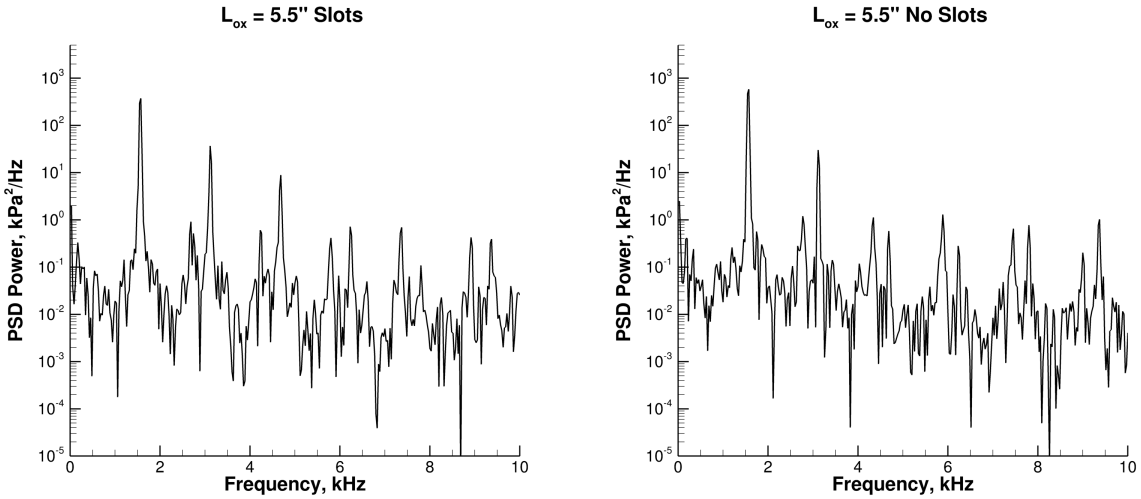

(a) Case 7: choked slots, 5.5 in.

(b) Case 8: no slots, 5.5 in.

Figure 6: PSD analysis for the three-dimensional simulations.

Table 4: Frequency and peak-to-peak pressure amplitudes for the three-dimensional cases and corresponding experimental operating point for the 5.5 in oxidizer post length.

Case	Mode	f, Hz	p'_{ptp}, kPa
Experiment	1	1324	387.15
	2	2655	89.29
	3	3979	46.37
7: Slots	1	1571	308.68
	2	3114	85.11
	3	4685	43.25
8: No-slots	1	1571	388.06
	2	3114	78.53
	3	4323	17.62

The peaks in the trough are the result of the wave in the oxidizer post returning to the backstep.[20] For the 5.5 in oxidizer post length this occurs approximately 60% of the way through the cycle. The behavior in the trough of the waves suggests that the reflecting wave in the oxidizer post is stronger in the constant mass flow case.

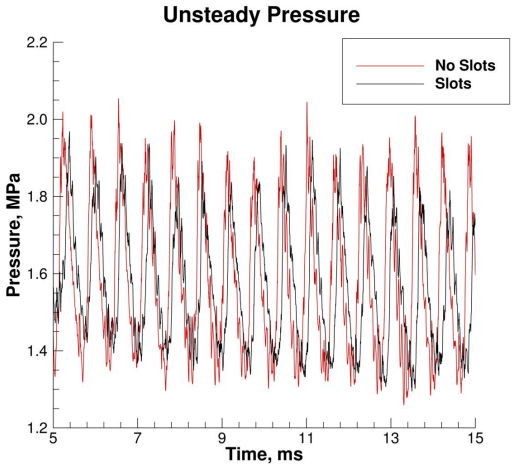

(a) 10 ms snapshot of the unsteady pressure.

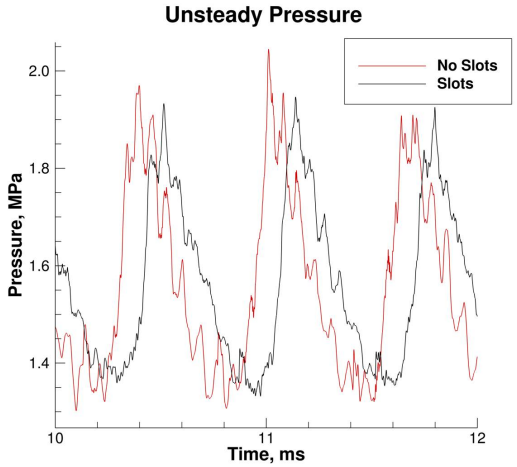

(b) Close-up view of the unsteady pressure showing the differences in the wave trough.

Figure 7: Unsteady pressure history taken at the combustor wall 1.25 cm from the backstep for the three-dimensional simulations.

C. Mode Shape

The acoustic mode shape is instructive because it is illustrative of the dynamic behavior of the flowfield. Figure 8 shows the mode shape for the pressure and Figure 9 shows the mode shape for the velocity. Both figures show the first three longitudinal modes. The mode shapes are a phase-averaged representation of the flowfield with each line representing a snapshot of a single cycle. Pressure mode shapes are normalized using the 14.5 in location and velocity mode shapes are normalized using the peak furthest downstream. Details on the computation of the mode shapes can be found in Ref 3.

Looking at the pressure mode shape for the first mode the two antinodes and single node in the combustor are predicted by both boundary conditions. Both simulations also show the bump near the backstep which is aligned with the location of the peak heat release. Feldman et al. showed that simulations with the slots provided excellent agreement with the experimental pressure mode shape for the first mode.[5] As expected in the region adjacent to the oxidizer inlet there are differences. The constant mass flow boundary shows a perfect antinode, while the choked slots push the antinode slightly downstream in the oxidizer post away from the inlet. The amplitude of the shifted antinode is slightly higher, 1.4 times the downstream amplitude compared with 1.2 times for the constant mass flow case.

The pressure mode shape for the second mode for the two configurations is again very similar, especially in the combustor. In the oxidizer post there are some differences. The slots again show a shifted node but this time the amplitude is lower, 3.4 times the downstream amplitude compared with 3.7 for the constant mass flow configuration. The antinode near -0.04 m also has a higher amplitude in the constant mass flow case, 4.5 compared with 4.0. The third longitudinal mode is very different for both configurations. In the oxidizer post multiple nodes and antinodes are visible for the choked slots, this is completely absent in constant mass flow case. The amplitude of the oxidizer post antinodes is also significantly different, nearly 7 times the downstream amplitude for the slotted inlet and of the same order as the downstream fluctuations without the slots. This shows that the higher harmonics are not well captured by the approximate constant mass flow boundary.

The velocity mode shape for the first two modes show higher velocity fluctuations near the oxidizer inlet for the slotted inlet, which is expected due to the unsteadiness of the region. The combustor mode shapes

are similar for the two configurations; both feature the expected 90° phase shift between the pressure and velocity in the combustor. Again, the third mode shows substantial differences; the amplitude of the velocity fluctuations in the oxidizer post are much lower for the constant mass flow inlet. The approximate inlet appears to have difficult in producing the higher-order harmonic behavior that is observed experimentally. Recall that the PSDs showed the amplitude prediction of the third mode was poor. In summary, we can therefore state that, for the constant mass flow inlet, the amplitude, frequency, and shape of the third mode is substantially different from the behavior predicted by the choked slots inlet.

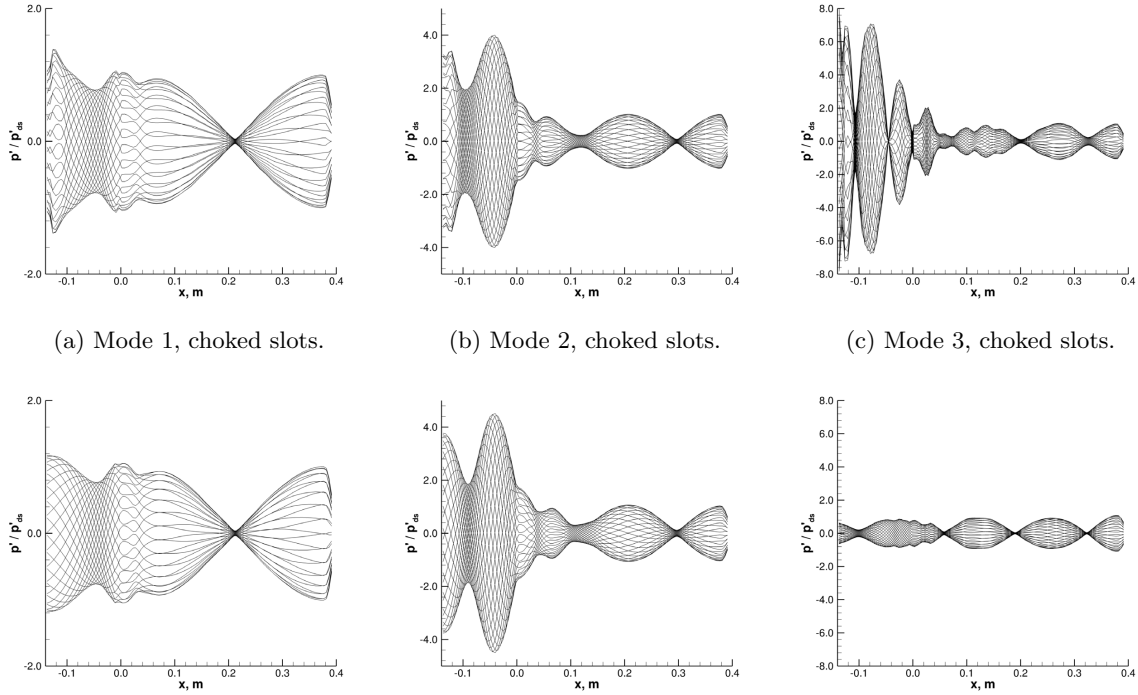

(a) Mode 1, choked slots. (b) Mode 2, choked slots. (c) Mode 3, choked slots.

(d) Mode 1, no slots. (e) Mode 2, no slots. (f) Mode 3, no slots.

Figure 8: Pressure mode shape for the first three modes for the cases with (a,b,c) and without (d,e,f) slots. In all plots the pressure has been normalized by the pressure at the 14.5 in transducer location.

D. Time-averaged Flowfield

While the mode shapes show the dynamic behavior of the instability, mean flow and multidimensional differences are not apparent. The time-averaged flowfield offers a single snapshot comparison of the two inlets. Shown in Figure 10 is the time-averaged flowfield for cases 7 and 8. With the exception of the area adjacent to the oxidizer inlet, the time-averaged flowfields are very similar. There is a low-pressure high Mach region resulting from the choked slots that is absent with the constant mass flow inlet boundary condition. This high Mach region extends 4.25 cm downstream of the slots; the flow subsequently becomes more uniform as it approaches the expansion into the combustor. The bulk flow Mach number just upstream of the expansion into the combustor is about 0.37 for both cases. The mean pressure in the combustor is slightly higher in the case without slots, 1565 kPa compared to 1540 kPa.

The temperature plot indicates that there is a difference in the recirculation region and heat release. In the constant mass flow case the temperature contour shows an outward bump near $x = 3.0$ cm. We also see that the oxidizer is present further downstream when using the choked slots, indicating that the heat release in the constant mass case is closer to the backstep.

The time averaged heat release and streamlines are plotted in Figure 11. The peak heat release is different in each case: for the constant mass flow inlet the peak heat release is higher and located closer to the backstep, which explains the difference in the O_2 distribution. There is also a region near $x = 3$ cm located directly in the recirculation region that has an elevated heat release, showing that more combustion

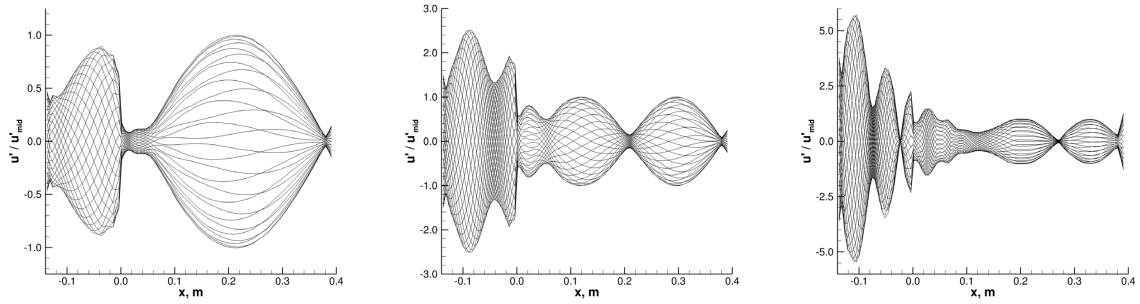

(a) Mode 1, choked slots. (b) Mode 2, choked slots. (c) Mode 3, choked slots.

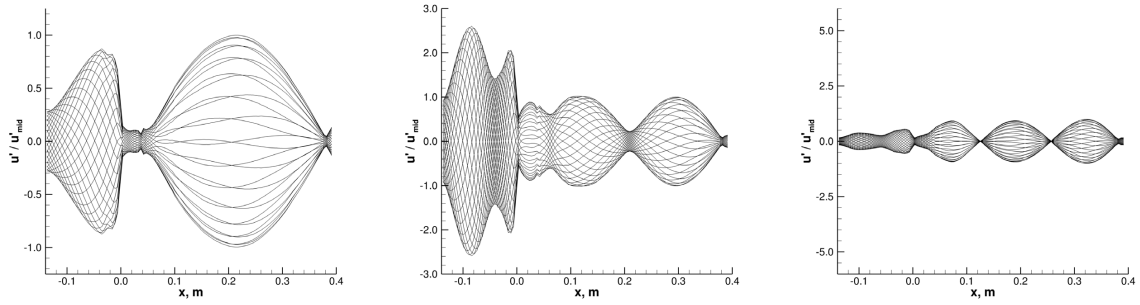

(d) Mode 1, no slots. (e) Mode 2, no slots. (f) Mode 3, no slots.

Figure 9: Velocity mode shape for the first three modes for the cases with (a,b,c) and without (d,e,f) slots. In all plots the velocity has been normalized by the furthest downstream peak velocity in the combustor.

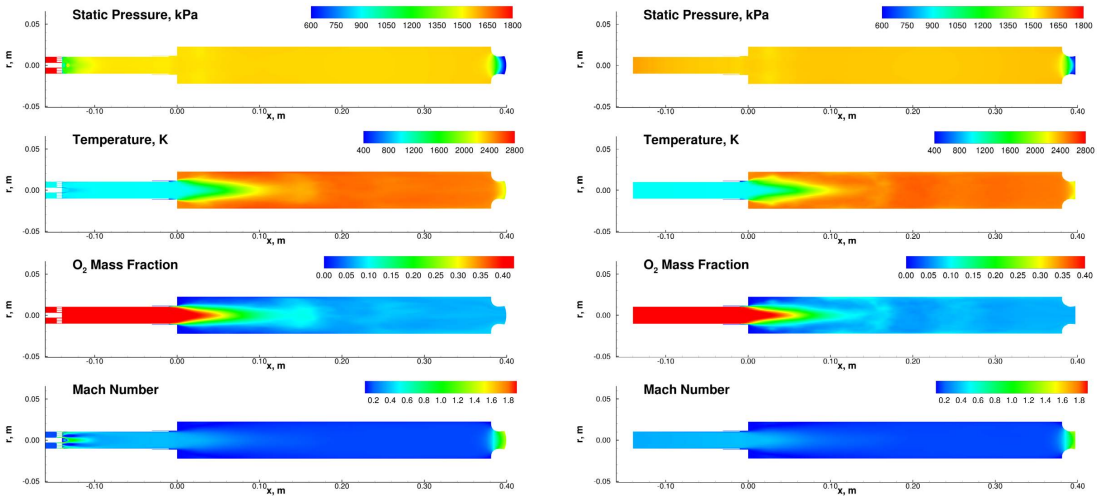

(a) Case 7: slots. (b) Case 8: no slots.

Figure 10: Slice through $z = 0$ for the three-dimensional simulations showing the time averaged flowfield. Time averaged flowfields show minimal circumferential variations.

is taking place in the recirculation region. This may indicate that the recirculation region is more strongly coupled with the heat release possibly giving rise to higher levels of instability. The recirculation regions are also different, with the reattachment point being located further downstream for the constant mass flow case.

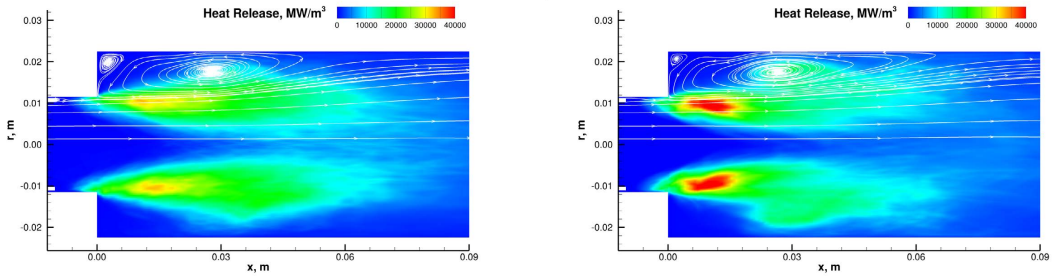

(a) Case 7: slots.

(b) Case 8: no slots.

Figure 11: Time averaged heat release and time averaged streamlines shown on a slice through $z = 0$. Time averaged three-dimensional results show minimal variations in the circumferential direction.

VII. Rayleigh Index

The Rayleigh index is a measure of how well correlated the pressure and combustion heat release oscillations are.[21] Mathematically the Rayleigh index is,

$$\mathscr{R} = \frac{1}{T}\int_{t_0}^{t_0+T}\int_V p'(\mathbf{x},t)\dot{q}'(\mathbf{x},t)\,\mathrm{d}\mathbf{x}\,\mathrm{d}t. \tag{7}$$

It is possible to consider a local Rayleigh index if we assume that the integration volume is the cell volume. Integrating over the individual cell volumes we obtain a formula for the local Rayleigh index,

$$\mathscr{R}(\mathbf{x}_i) = \frac{1}{T}\int_{t_0}^{t_0+T} p'(\mathbf{x}_i,t)\dot{q}'(\mathbf{x}_i,t)\,\mathrm{d}t. \tag{8}$$

Positive values of the local Rayleigh index correspond to regions, where the pressure and combustion heat release are in phase and amplify the instability. On the other hand, regions where the index is negative damp the instability. A plot of the local Rayleigh index for a cycle is shown in Figure 12. The slot boundary case shows a positive Rayleigh index starting just upstream of the backstep and extending into the combustor in the shear layer. The center of the flow is largely void of the peaks. The recirculation region shows small regions of damping. Beyond the 5 cm location the, peaks (both positive and negative) are small and localized. For the case without slots there is active driving in the shear layer again but extends further downstream and inward towards the center of the combustor. The regions of damping are also smaller and there are still large regions of driving past the 5 cm location.

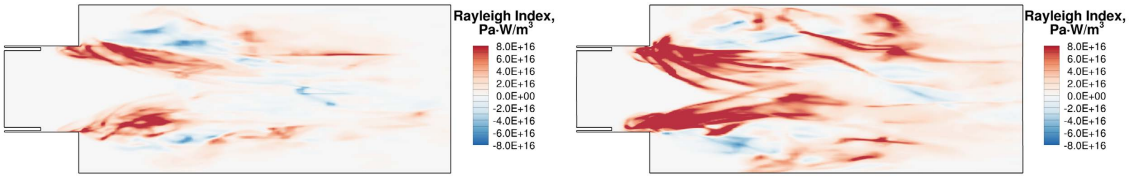

(a) Case 7: slots.

(b) Case 8: no slots.

Figure 12: Local Rayleigh index for a single cycle for the three-dimensional simulations. Region shown is a slice through $z = 0$ extending 10 cm past the backstep.

It is perhaps surprising that the Rayleigh index plots are markedly different for the two boundary condition treatments, when the acoustic modes and PSDs are reasonably close. The difference may be attributed to different heat release contours, a feature that was evident in the time-averaged heat release results shown earlier, In order to understand the underlying reasons for the different heat release distributions, we look at the vorticity results from the two cases.

The plot of the vorticity near the slots shown in Figure 2 showed a large amount of vorticity generated from shedding vortices at the slots. To investigate if this difference persists into the combustion region the time averaged vorticity magnitude near the combustion region is plotted in Figure 13. An exaggerated scale is used to highlight the differences in the center of the chamber while masking the peak values in the boundary layer. For the configuration without slots the vorticity in oxidizer post is largely only present near the wall and is due to generation of vorticity in the boundary layer; a low vorticity core is present in the combustor. In contrast the slot configuration shows evidence of a measurable amount of vorticity in the center of the oxidizer post. In this case, the shed vortices from the slots travel further downstream and persist in the combustor. It is known that vortex impingement can amplify acoustic pressure fluctuations.[22,23] The greater levels of vorticity may contribute to a higher degree of mixing, and perhaps lead to more uniform combustion heat release over the pressure cycle. This may be the reason why the Rayleigh index shows lower levels of pressure-heat release correlation. These findings suggest that the appropriate treatment of inlet boundary effects may in fact have profound effects on the heat release and acoustic coupling phenomena. More extensive studies of these features are warranted before definitive conclusions can be drawn.

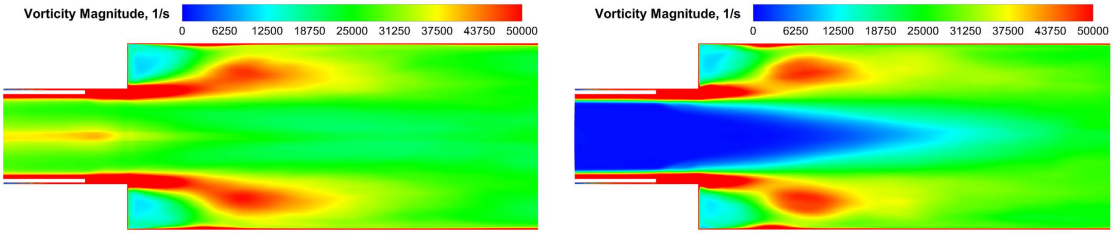

(a) Case 7: slots.

(b) Case 8: no slots.

Figure 13: Time averaged vorticity plotted on an reduced scale to highlight differences in the center of the oxidizer post. Region shown is a slice through $z = 0$, the plotted region starts 3 cm upstream of the backstep and extends 10 cm past the backstep.

VIII. Summary

The accurate treatment of boundary conditions can be of significance for the prediction of acoustic modes and combustion instabilities in rocket combustors. Approximate boundary treatments are often desirable in order to limit the extent of the domain that must be modeled. In this study, two inlet boundary conditions have been evaluated for an experimental longitudinal mode combustor that is capable of sustaining high-amplitude combustion instabilities. These include the actual complex choked slot boundary used in the experimental configuration and a constant mass flow boundary condition that approximates the choked flow inlet. Both 2D and 3D studies are used to elucidate the key differences between these two boundary treatments. The 2D studies of both stable and unstable operating points show that significant differences are apparent and, in general, the constant mass flow boundary is observed to generate higher levels of instability, especially for the first mode.

Three-dimensional simulations of an unstable configuration show better agreement in the overall PSD predictions of the two cases. The acoustic mode shapes of the first two modes are also correctly predicted. However, the constant mass flow inlet displays higher levels of instability and does not correctly predict the third (and higher) harmonic modes. Also, the amplitude of the first mode is observed to be higher for the approximate boundary treatment. An examination of the Rayleigh index further shows a different pattern of regions that drive the instability. The underlying reason appears to be the differences in the vorticity field, which in turn lead to different levels of mixing and heat release distributions. More detailed studies are needed to elucidate these phenomena. It may also be possible to use the results from the complete geometry

to generate a more realistic conditions for the approximate boundary. In conclusion, we note that some aspects of the flowfield such as the first two acoustic modes are well captured, while other features such as the heat release distribution and higher harmonic modes are not as well-represented. This suggests that such boundary condition approximations must be used judiciously, perhaps in combination with more detailed boundary studies to ascertain that the essential aspects are correctly predicted.

Acknowledgments

The authors wish to thank Thomas Feldman of Purdue University for providing the experimental data. Computing resources were provided by the DoD High Performance Computing Modernization Program.

References

[1]Yu, Y., Sisco, J., Rosen, S., Madhav, A., and Anderson, W., "Spontaneous Longitudinal Combustion Instability in a Continuously-Variable Resonance Combustor," *Journal of Propulsion and Power*, Vol. 28, No. 5, 2012, pp. 876–887.

[2]Feldman, T., *Unstable Combustion Processes for a Single Element Shear/Coax Injector in a Longitudinal Combustor*, Masters thesis, Purdue University, West Lafayette, May 2013.

[3]Harvazinski, M., *Modeling Self-Excited Combustion Instabilities Using a Combination of Two- and Three-Dimensional Simulations*, Dissertation, Purdue University, West Lafayette, May 2012.

[4]Harvazinski, M., Anderson, W., and Merkle, C., "Analysis of Self-Excited Combustion Instability using Two- and Three-Dimensional Simulations," *Journal of Propulsion and Power*, Vol. 29, No. 2, 2013, pp. 396–409.

[5]Feldman, T., Harvazinski, M., Merkle, C., and Anderson, W., "Comparison Between Simulation and Measurement of Self-Excited Combustion Instability," *48th AIAA/ASME/SAE/ASEE Joint Propulsion Conference and Exhibit*, AIAA, Atlanta, GA, July 2012.

[6]Smith, R., *Computational Investigation of High Frequency Acoustics and Instabilities in a Single-Element Rocket Combustor*, Ph.D. thesis, Purdue University, West Lafayette IN, Aug 2010.

[7]Smith, R., Xia, G., Anderson, W., and Merkle, C., "Computational studies of the effects of oxidizer injector length on combustion instability," *Combustion Theory and Modeling*, Vol. 12, 2012, pp. 341–368.

[8]Garby, R., Selle, L., and Poinsot, T., "Large-Eddy Simulation of Combustion Instabilities in a Variable-length Combustor," *Comptes Rendus Mécanique*, Vol. 341, No. 1-2, 2013, pp. 220–229.

[9]Guézennec, N. and Mennon, S., "Large-Eddy Simulation of Combustion Instability in a High-Pressure Shear-Coaxial Injection Combustor," *Submitted to Combustion and Flame*, 2013.

[10]Lian, C., Xia, G., and Merkle, C., "Solution-Limited Time Stepping to Enhance Reliability in CFD Applications," *Journal of Computational Physics*, Vol. 228, 2009, pp. 4836–4857.

[11]Lian, C., Xia, G., and Merkle, C., "Impact of source terms on reliability of CFD algorithms," *Computers & Fluids*, Vol. 39, 2010, pp. 1909–1922.

[12]Li, D., Sankaran, V., Merkle, C., and Lindau, J., "A Unified Computational Formulation for Multi-Component and Multi-Phase Flows," *43rd AIAA Aerospace Sciences Meeting and Exhibit*, January 2005, AIAA Paper 2005-1391.

[13]Li, D., Xia, G., Sankaran, V., and Merkle, C., "Computational Framework for Complex Fluids Applications," *3rd International Conference on Computational Fluid Dynamics*, Toronto, Canada, July 2004.

[14]Spalart, P., Jou, W., Strelets, M., and Allmaras, S., "Comments on the feasibility of LES for wings on a hybrid RANS-LES approach," *1st U.S. Air Force Office of Scientific Research Office Conference on DNS/LES*, Columbus, OH, August 1997, pp. 137–148.

[15]Travin, A., Shur, M., and Splart, P., "Physical and numerical upgrades in the detached-eddy simulation of complex turbulent flows," *412 EUROMECH Colloquium on LES of Complex Transitional and Turbulence Flows*, Munich, October 2000.

[16]Wilcox, D., *Turbulence Modeling for CFD*, DCW Industries, 1998.

[17]Wilcox, D., "Formulation of the k-ω turbulence model revisited," *45th AIAA Aerospace Sciences Meeting and Exhibit*, AIAA, Reno, NV, January 2007.

[18]Westbrook, C. and Dryer, F., "Simplified Reaction Mechanisms for the Oxidation of Hydrocarbon Fuels in Flames," *Combustion Science and Technology*, Vol. 27, 1981, pp. 31–43.

[19]Jones, W. and Lindstedt, R., "Global Reaction Schemes For Hydrocarbon Combustion," *Combustion and Flame*, Vol. 73, No. 3, September 1988, pp. 233–249.

[20]Harvazinski, M., Huang, C., Sankaran, V., Feldman, T., Anderson, W., Merkle, C., and Talley, D., "Combustion Instability Mechanisms in a Pressure-coupled Gas-gas Coaxial Rocket Injector," *49th AIAA/ASME/SAE/ASEE Joint Propulsion Conference (JPC)*, AIAA, San Jose, CA, July 2013.

[21]Rayleigh, J., "The Explanation of Certain Acoustical Phenomena," *Nature*, Vol. 18, 1878, pp. 319–321.

[22]Schadow, K. and Gutmark, E., "Combustion instability related to vortex shedding in dump combustors and their passive control," *Progress in Energy and Combustion Science*, Vol. 18, No. 117, 1992.

[23]Schadow, K., "Combustion Dynamics: Passive Combustion Control," *Active Control of Engine Dynamics*, No. RTO-EN-020, NATO, Brussels, Belgium, May 2001.